Mechanics of Fibroblast Locomotion: Quantitative Analysis of Forces and Motions at the Leading Lamellas of Fibroblasts

Stephen Felder and Elliot L. Elson

Department of Biochemistry and Molecular Biophysics, Washington University School of Medicine, St. Louis, Missouri 63110

Abstract. Shapes, motions, and forces developed in lamellipodia and ruffles at the leading edges of primary chick embryo heart fibroblasts were characterized by differential interference contrast microscopy and digital video enhancement techniques. The initial extension of the cell edge to form a thin, planar lamellipodium parallel to the substrate surface was analyzed in two dimensions with temporal and spatial resolution of 3 s and 0.2 μm, respectively. An extension begins and ends with brief, rapid acceleration and deceleration separated by a long period of nearly constant velocity in the range of 4–7 μm/min. Extensions and retractions were initiated randomly over time. As demonstrated by optical sectioning microscopy, the extended lamellipodia formed ruffles by sharply bending upward at hinge points 2–4 μm behind their tips. Surprisingly, ruffles continued to grow in length at the same average rate after bending upward. They maintained a straight shape in vertical cross section, suggesting the ruffles were mechanically stiff.

The forces required to bend ruffles of these cells and of BC3H1 cells were measured by pushing a thin quartz fishpole probe against the tip of a ruffle 7–10 μm from its base either toward or away from the center of the cell. Force was determined by measuring the bending of the probe monitored by video microscopy. Typically the probe forced the ruffle to swing rigidly in an arc about an apparent hinge at is base, and ruffles rapidly, and almost completely, recovered their shape when the probe was removed. Hence, ruffles appeared to be relatively stiff and to resist bending with forces more elastic than viscous, unlike the cell body. Ruffles on both types of cells resisted bending with forces of 15–30 μdyn/μm of displacement at their tips when pushed toward or away from the cell center. The significance of the observations for mechanisms of cell locomotion is discussed.

MIGRATION of fibroblasts and fibroblast-like cells over a flat surface seems to occur as a cyclic process with two major phases (Abercrombie et al., 1970*a*,*b*; Trinkaus, 1984). First the cell extends a thin lamellipodium from its leading edge that contacts the substrate. Then portions of the cell behind the lamellipodium are drawn forward. During this cycle on some substrates, the extended lamellipodium is sometimes drawn backward to form a "ruffle."

Although much information has been obtained about locomotion of diverse kinds of cells, the mechanisms by which the processes are coordinated and force is developed are still unknown (Trinkaus, 1984). Some investigators have suggested that cytoskeletal functions such as polymerization of filaments and myosin-dependent contractibility provide the driving forces for cellular locomotion (Abercrombie et al., 1977; Small, 1982; Rinnerthaler et al., 1988; Smith, 1988; Mitchison and Kirschner, 1988; Bray and White, 1988). Others have proposed that forward motion results from polarized deposition of cell surface membrane at the leading edge of the cell (Abercrombie et al., 1970*c*; Bretscher, 1984; Kupfer and Singer, 1988). The objectives of the work presented here are to describe fine details of leading edge motions and to measure forces generated in this region. This information sheds light on the mechanics of these processes and how they may be involved in cell locomotion.

The general characteristics of the extension and retraction processes have previously been identified for fibroblasts (Abercrombie et al., 1970*a*; Chen, 1979, 1981) and for epithelial cells (Dipasquale, 1975). Motions of the leading edges of cells were studied by following the positions of a small number of discrete points along the active edges in time lapse images of cells taken at 0.5- or 1-min intervals. These studies, however, viewed only a two-dimensional projection of three-dimensional processes that often involve the folding and elevation from the substrate of motile lamellas to form ruffles. Observations of motile cells from a lateral view have yielded insights into the movement of ruffles in the vertical plane (Ingram, 1969), but were limited in spatial resolution, and were not quantitative. Alternatively, the three-dimensional shapes of ruffled extensions have been viewed by electron microscopy (Abercrombie et al., 1972). These studies allow excellent visualization of the

S. Felder's present address is the Department of Molecular Biology, Rorer Biotechnology, Inc., King of Prussia, PA.

structures, but not analysis of their movements. In addition, the observed shapes, especially of thin ruffles, may be perturbed by fixation or freezing. We have used high resolution differential interference contrast video microscopy and optical sectioning to characterize the two- and three-dimensional motions of the leading edges. These techniques have allowed us to surpass the temporal and spatial resolution of the earlier observations of live cells.

We have found that extension of the lamellipodium occurs smoothly, directly, and with constant velocity. As the lamellipodium continues to grow in length, it lifts upward to form a ruffle. In swinging up from the substratum the ruffle bends about a localized hinge point 4–6 μm behind its extending tip. Interestingly, the ruffle continues to extend or grow in length at nearly the same rate after it has bent upwards. The elevated, extending portion of the ruffle distal to the hinge is mainly straight in cross section suggesting that its shape is rigidly maintained by its internal structure. We have found no evidence that extension and ruffling retraction occur with regular periodicity in time as previously suggested (Abercrombie et al., 1970*a*).

These results suggest that ruffles are relatively stiff structures. To test this suggestion, we have used fine quartz fibers to measure the stiffness of ruffles. The sensitivity of the fibers allowed measurements of forces in the range of 3–100 μdyn. This approach has previously been used in different applications (Evans et al., 1980; Howard and Hudspeth, 1987; Kishino and Yanagida, 1988). We report that ruffles are indeed very stiff considering their thinness, and are largely elastic. Upon being pushed, they remain straight and bend at a point near their bases, resisting deformation with forces of 15–30 μdyn/μm displacement of their tips. Our results provide a context for and place constraints on mechanistic models of fibroblast locomotion.

Materials and Methods

Cells and Tissues Cultures

Primary explant cultures of chick embryo heart fibroblasts (CHFs)[1] were used for measurements of ruffle deformability and for observations of motions and were prepared as follows (Izzard and Lochner, 1976). Hearts were removed from 8- to 10-day-old chick embryos and rinsed with TBS. The hearts were cut into small (~1-mm) pieces with a microdissection scissors; the pieces were rinsed in TBS and allowed to settle; and the TBS was removed. Rinsed pieces were resuspended in primary growth medium (Hunter, 1979) consisting of DME with 8% FCS, 2% chick serum, and 10% tryptose phosphate broth, and were placed on 22 × 22-mm cover slips in 35-mm tissue culture dishes. CHF tissue chunks in primary growth medium were cultured overnight in a 5% CO_2 incubator at 37°C, and fibroblasts that had migrated out of the tissue chunks onto the coverslip to a form a ring of cells around the chunks after 15 h were used. BC3H1 cells are a smooth musclelike cell line (Schubert and Harris, 1974). These were grown in BC3H1 medium which retained the cells in an undifferentiated state and consisted of high glucose DME supplemented with 20% FCS in a 5% CO_2, 37°C incubator. Logarithmically growing cells half way to confluency were used for measurements of ruffle deformability.

To characterize leading lamellar motions, a Teflon O-ring (Millipore Continental Water Systems, Bedford, MA) was coated with vaseline and placed onto a microscope slide, and the cavity thus created was filled with culture medium in a 5% CO_2 environment. A coverslip with attached cells was placed face down onto this Teflon ring. The resulting sealed chamber had a volume of ~50 μl. Cells in this chamber were observed for up to 1 h, and continued to ruffle and migrate actively for at least 2 h.

To measure ruffle bending forces coverslips with attached cells were removed from culture medium and sealed with vaseline to the bottom (outside) of 35-mm plastic tissue culture dishes in which 15-mm-diam holes had been drilled, so as to leave the cells of the center region of the coverslips exposed and accessible to the inside of the dish. The dishes were filled with the appropriate culture medium for the two cell types, supplemented with 20 mM Hepes to maintain the pH at 7.4.

Digital Video Microscopy

Cells were viewed with a Zeiss IM35 inverted microscope and 63× planapochromat oil immersion objective (NA of 1.4). For motion analysis, Normarski differential interference optics (oil immersion condensor with NA of 1.4) were used; for force measurements, cells and fishpole probe were viewed with phase three illumination from a long (9-mm) working distance condensor with NA of 0.6.

Images of the cells were collected with a vidicon video camera with aspect ratio adjusted to yield equal magnification in two dimensions and digitized by a Grinnell GMR 274 video frame buffer. A 6.3× eyepiece was placed between the microscope and the video camera to increase magnification. Under these conditions, the total magnification was such that the full video screen width displayed 90 μm. Four or eight video frames were averaged within the video frame buffer to decrease video noise, and up to 1,000 averaged frames were stored by use of a VAX 11/780 computer onto an RM80 disk at 3.0- or 6.0-s intervals (motion experiments) or at 1.0-s intervals (force experiments). Maximally one full frame of video data (0.25 megabytes) could be stored per second. The microscope and video camera were placed on a vibration isolation table (Kinetic Systems, Inc., Boston, MA). The microscope stage, condenser, and objectives were enclosed in a Plexiglass box with a total volume of ~1.5 cubic feet. A slow stream of warm air was blown into the box to maintain an ambient temperature of 36.5°C. For the force measurements, the video signal was also recorded directly from the camera onto a time lapse video tape recorder (Panasonic NV8040) to assess the effect of the deformations on the ability of the cells to continue ruffling.

Two-dimensional Edge Analysis

The edge of the cell (i.e., the border of the two-dimensional projection of the cell onto the focal plane of the microscope) was identified by hand for the first image frame of the time sequence. The cursor supplied in the video frame buffer system was used to designate points along the cell's edge. The edge of the cell for each successive frame in the sequence of up to 500 frames was then identified automatically by a computer algorithm developed specifically for this analysis involving pattern recognition and image registration. The algorithm has been presented in detail (Felder, 1984).

Displacement Data

Detailed motions of the cell edge were characterized using radial lines intersecting the edge as local coordinate axes. For round cells, the radii originated from the average center of mass of the projected cell outline. For cells with elongate shapes, radial lines were described for each region of the cell at which the edge was actively extending and retracting. These radial lines originated from the center of curvature of an arc that approximated the average shape of the region's active edge. The points of intersection of the edge at the time with each radial line were identified by computer program, and the distance outward along the radial line from the local center to the point of intersection was calculated. The average distance along each radial line for all frames analyzed was subtracted from each measured distance. The resultant displacement data set provided the distance from the average edge position outward along radial lines as a discrete function of time (or frame number) and radial position. The duration of the data records ranged between 600 and 3,000 s (200 to 500 data points), with the sampling rate of 1 frame/3.0 or 6.0 s.

Optical Sectioning Microscopy

Optical sectioning was performed manually by moving a rod affixed to the fine focus control along a notched surface (for details, see Felder, 1984). The uncertainty of the amount of elevation for each position was estimated to be 0.15 μm. A video image of the cell (usually 150 × 150 pixels in size) was collected at each focal plane at 0.5- or 1.0-s intervals. The first image recorded the focal plane at the base of the cell. Then the objective was quickly moved by a unit step size of either 0.5 or 1.0 μm, and the next image was recorded at this new focal plane. Successively higher (more dorsal),

1. *Abbreviation used in this paper*: CHF, chick embryo heart fibroblasts.

focal planes were recorded until the highest point of the cell was in focus. Then the focus was rapidly returned to the level of the base of the cell and the process was repeated. Typically 8 or 10 focal planes were recorded per cycle and two time intervals were used to refocus to the base of the cell at the end of each cycle. The images from a full cycle together make up one "time frame" of optical sectioning data. Between 10 and 35 time frames were collected for each cell.

Cross-sectional Shapes and Lengths of Ruffles

To analyze the shape of the ruffles in cross section, lines were drawn by eye perpendicular to the ruffling edge of the cell at ~2 μm intervals. The image of each focal plane for each time frame was scanned along this line (Felder, 1984), and the point of largest absolute difference from the background intensity level was identified by computer as being the likely point of intersection of the cross-sectional line with the ruffle. The estimated intersection points for each line were inspected by use of a computer program that displayed to the user the image, the point chosen, and the line scanned. Corrections were made when necessary, and were required mostly for the lowest level frame where other bright or dark spots appeared due to other structures inside the cell. The result was a set of points that when connected identified the intersection of the ruffle with a vertical plane of cross section.

The length of the ruffle along this plane of cross section was calculated by summing the lengths of line segments connecting the points of intersection between the ruffle and the plane for consecutive optical sections. The sum was begun at an arbitrary starting point inside the cell on the cross-sectional line within the "lowest" focal plane (so the offset of the values was arbitrary). Pictorially, the lengths of line segments of data similar to that plotted in Fig. 5 were summed. Since the resolution in the dorsal-ventral direction was 1 μm, the uncertainty in length measurements was high. This is estimated to be 0.7 μm for nearly vertical ruffles, and 1.5 μm for ruffles bent upwards at an angle of 30°. The defined lengths for the first six time frames (50 s) after the ruffle first was observed to lift from the substrate were fit to straight lines by linear regression. The fitted slopes for four to six vertical sections were averaged, yielding the estimated velocity of growth and its standard deviation. The correlation coefficients were >0.8, and the total increase in length during the 50-s period averaged 4 μm, and hence exceeded the estimated uncertainty of the measurement by three to sixfold. The rate at which the base of the cell retracted after the ruffle had lifted was calculated by fitting the length of the cell within the "lowest" (nearest the substrate) optical section in the same way. For both calculations of rates, the frame at which the extending tip first appeared in the second optical section was the first time frame used. This eliminated possible errors in comparing length of the ruffle before and after lifting, and removed the rapid decrease in extension of the base of the cell that was due to the rapid bending upward of the extended lamellipodium that usually occurred at a point 2–4 μm behind the extending tip.

To reconstruct the shapes of the ruffles in cross section, intersection points between ruffle and vertical planes for consecutive optical sections were connected by straight lines. First, however, the intersection points were corrected for time lags between the collection of the lower and upper images within a time frame. We assumed that the ruffle moved steadily and parallel to the cross-sectional line between time frames. The corrected position of the ruffle at each focal plane level was calculated by linear interpolation, preceding time frame to current time frame, in accord with the respective time delay.

Quartz Fishpole Probes

Quartz fishpole probes were produced following the specifications for constructing balances capable of weighing samples of 1–10 ng (Lowry and Passonneau, 1972). Quartz fibers of 3-mm diameter were flame blown to lengths of 5–10 cm with diameters ranging from 0.3 to 1.5 μm. One fiber estimated to be 0.5 μm in diameter was selected for use. The fiber was secured at one end to a Pasteur pipette and was cut to a free length of 2.94 ± 0.06 mm. The sensitivity (resistance to bending) of this fiber was calibrated by hanging pieces of individual freeze-dried muscle tissue on the tip of the horizontal quartz fiber, and measuring the deflection of the tip, which ranged from 0.3 to 0.8 mm with a 70× dissecting microscope. The tissue samples ranged from 1.5 to 4 ng and were weighed on a previously calibrated fishpole balance as described (Lowry and Passonneau, 1972). The sensitivity was found to be 3.73 ± 0.18 (SEM) μdyn/mm.

Two lengths were cut from this fiber and mounted with epoxy onto the tips of glass micropipettes (see Fig. 9 [Appendix I]). The free lengths of the fibers were 282 and 421 μm. During the experiment, the position of the micropipette and hence the fishpole probe was controlled by a micromanipulator (Narishige Scientific Instrument Laboratory, Tokyo, Japan).

Collection of Force Data

The quartz fishpole probe was introduced into the dish at an angle of ~15° from horizontal, and cells and probe were located and manipulated into place under low power by moving the sliding microscope stage and the micromanipulator. The entire length of the quartz fiber was submerged. Video frame collection was run continuously to obtain 350 frames at 1-s intervals while a cell was being probed. A ruffle or microspike was brought into focus. The probe tip was then slowly brought into contact with the ruffle 7–10 μm above the coverslip by use of the joystick control of horizontal and vertical positioning of the micromanipulator. Then the probe was moved horizontally, perpendicular to its long axis at a rate of 5–10 μm/s against the ruffle by use of the dial control of one horizontal dimension, also available on the micromanipulator. This insured as well as possible that the only movement of the fishpole was perpendicular to its length. Part of the dispersion of measured deformation forces might be due to the exertion of force by the probe in a direction not entirely normal to the probe length. The moored end of the probe was moved 10 to 30 μm during exertion of force, and so components of the motion not orthogonal to the probe length should be very small. Further, movement of the probe tip due to cell motion, being much smaller than the amount by which the moored end was moved, had little effect on the amount of force exerted.

Analysis of Force

During a measurement, the fishpole probe was held fixed at one end while the force of its interaction with the ruffle was perpendicular to the axis of the probe at its other end. The equation that relates the force on the probe to the magnitude of its resulting small deflection is derived in Appendix I. The applied force f (in μdyn) at the fishpole tip is related to the angular deflection, θ, at the tip for a short fiber segment of length l (in micrometers) cut from the calibrated stock fiber of length L (in millimeters) by:

$$f = -2/3\ (L/l)^3\ 3.73\ \sin\theta\ \mu\text{dyn}.$$

For the two segments used in these measurements this equation reduced to:

$f = 795 \pm 71 \sin\theta$ μdyn (for the 282 μm segment); and

$f = 357 \pm 32 \sin\theta$ μdyn (for the 421 μm segment).

The uncertainties in the calibration of f are due to uncertainties in length measurements and in the calibration of the stock fiber.

The angle that the tip of the fishpole probe made with respect to the video reference frame (coordinates fixed relative to the video camera) for each digitized video image was calculated as follows. The coordinates in the video reference frame of five points estimated to lie along the center of the beam and to range from 0 to 20 μm from the tip of the beam were identified by using the zoom and pan cursor feature of the Grinnell video frame buffer. These points were fit by linear regression to straight lines. In all experiments, the correlation coefficient was good (>0.97 or <−0.97).

A consecutive sequence of image frames was chosen for analysis when the first frame showed the probe to be apparently touching the cell but with no force exerted on the probe detectable in the angle measurement. Then, the next one or more frames captured time points at which the probe pushed against the ruffle. The force exerted on the probe in each frame of a sequence was calculated as explained above from the difference in tip angle for that frame minus the tip angle for the first (0 force) frame. The deformation of the cell structure was measured by the amount of movement of the probe tip perpendicular to its unstressed long axis.

The accuracy of the difference angle measurements was tested by recording video frames of the fishpole probe in position above and out of contact with the cells (unstressed) intermittently for 350 s. Short sequential segments of this data record were analyzed to yield the amount of angle variation. The average difference between the angle at one time point and the angle at a time point 1–10 s later was 0.0052 ± 0.0053 radians for the longer (more sensitive) fishpole probe. This uncertainty in the measurement of the difference angle translates to an uncertainty in the measurement of the force of 4.1 μdyn. The forces measured in experiments ranged between 4 and 60 μdyn, with an average of 34 μdyn, yielding an average signal to noise ratio of 9. The accuracy of the measurement of deformation, i.e., the extent of deflection of the probe tip, was estimated to be ± 1 pixel, or ± 0.2 μm. Accounting for estimated error in both force and displacement measurements, a force measurement of 35 μdyn with a displacement of 1.0 μm

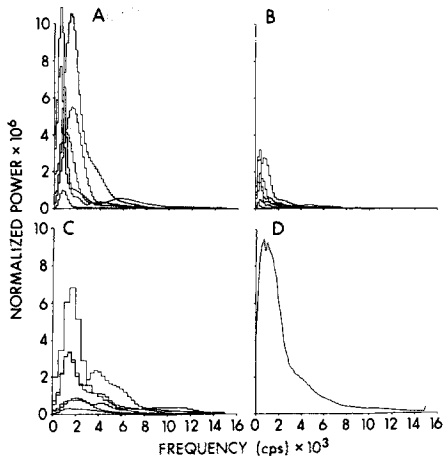

Figure 1. Power spectra of displacement data. The average power spectra for displacements as a function of time along radial lines of the active edge of each cell. (*A–C*). Each panel presents the average spectra for six cells. The overall average power spectrum for all 18 cells is shown in *D*. The spectra of *A–C* were weighted equally.

would have an expected uncertainty of 9 μdyn/μm. It was not possible to measure repeatedly the force of deformation of one ruffle to determine directly the uncertainty of the measurement because the ruffles change shape over time. Nevertheless, from an examination of the apparent linearity of the measurement seen when two or three measurements were performed on the same ruffle (see Discussion or Fig. 3), the uncertainty of the measurement must have remained in this range.

The sensitivity of the probe for this experimental design could be adjusted to range down to 1 μdyn and up to many mdyn. The limit in sensitivity results from the limit of making (and working with) quartz fibers thinner than ~0.2 μm, as well as from the fact that the amount of sway in the fiber due to fluid motions of the culture medium prohibits 0.2-μm-diam fibers longer than ~150 μm. A fiber sensitive to 1 μdyn/μm of displacement with an expected uncertainty in force measurements of 0.4 μdyn would have to be 0.2 μm in diameter and 120 μm long. This thinner fiber would be more difficult to calibrate, however.

Results

Two-dimensional Displacement Data

Displacement data records were developed for 18 cells. These records consisted of the measured distance outward of the leading, active edges of the cells as a function both of position along the edge and of time. To determine whether lamellipodial extensions showed a tendency toward oscillatory behavior, we calculated the average power spectrum for the displacement data records (Fig. 1). The shape of the average power spectrum, shown in Fig. 1 *D*, is consistent with a random, band-limited process, with power damped to half maximal at a frequency of 0.025 Hz. No significant secondary peaks were seen. Hence, although these processes may appear to occur at regular intervals (Abercrombie et al., 1970*a*), no oscillatory behavior was detected.

Rate and Time Course of Extension

The characteristics of larger lamellipodial extensions were determined by analyzing edge displacement data selected by two different sets of criteria. The first selected edge regions at least 1 μm wide that extended at least 2.5 μm over a period of at least 15 s (Fig. 2 *A*). Alternatively ruffling extensions were selected by visual inspection of the time lapse digital images. For 12 cells, all large ruffling events seen during data collection were analyzed and yielded 20 displacement records (Fig. 2 *B*). Data selected by the former, objective criteria did not differ from those selected by the latter, subjective criteria.

The behavior of the individual lamellar extensions shown in Fig. 2, (*A* and *B*) is summarized in Fig. 2 *C*, which presents a histogram of the rates of edge extension. These values agree well with those found earlier for fibroblasts (Abercrombie et al., 1970*a*) and epithelial cells (Dipasquale, 1975) and for the extension of filopodia from nerve growth cones (Argiro et al., 1985). Altogether 71 periods of extension were catalogued. All these events occurred smoothly

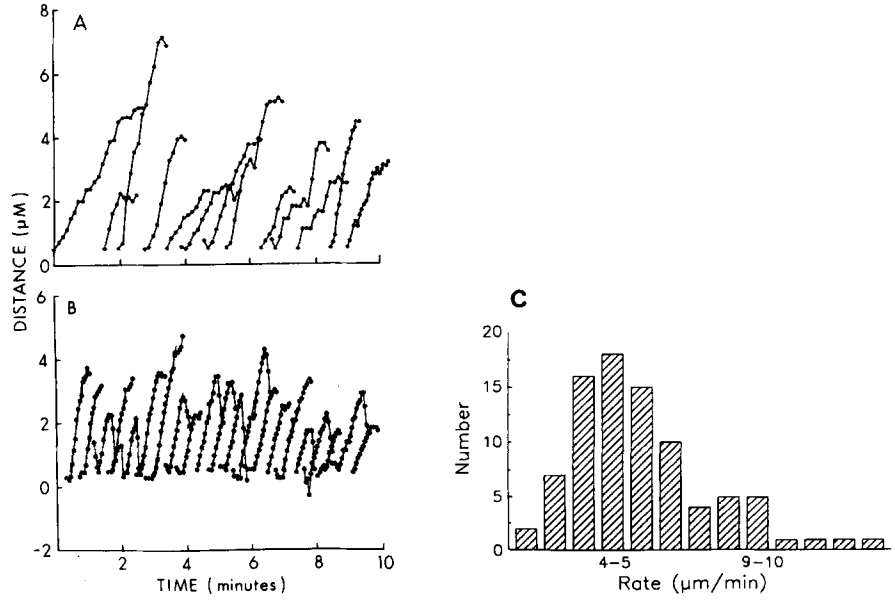

Figure 2. Rate and time course of extension. Events were selected from the full-time course displacement records for the 18 cells as described in the text. *A* and *B* present the displacement data directly for several individual extensions. Each extension drawn represents a different lamellipodium observed for one of the observed cells. The individual extensions are drawn to the same scale in time and displacement. *B* includes lines calculated by linear least squares fit to demonstrate the nearly constant velocity of extension. A histogram of the rates of 86 extension events is presented in *C*.

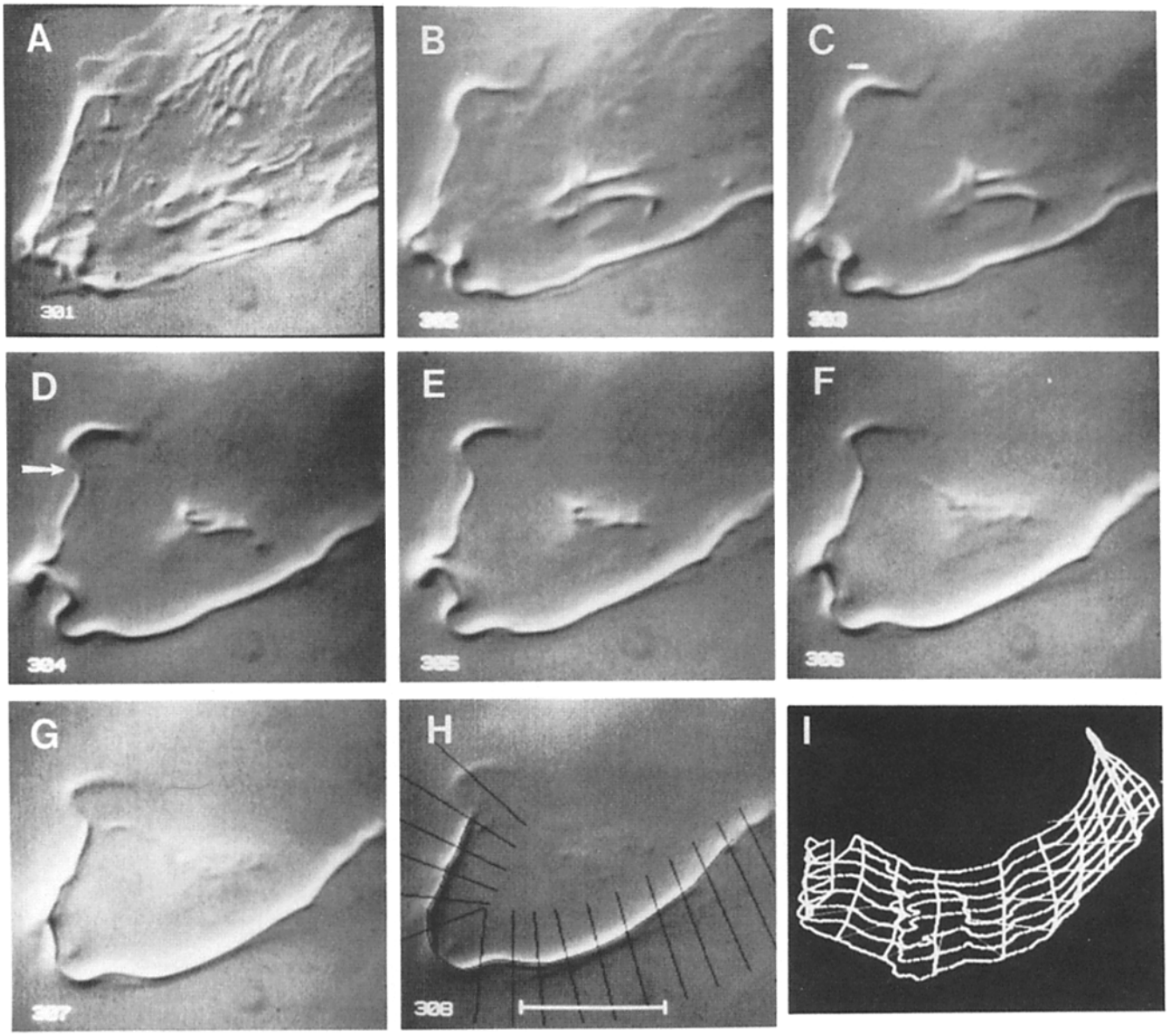

Figure 3. Raw optical sectioning image data. The digital image data for each focal plane for one time frame of data was photographed from the TV monitor. Pictured is a 30 × 30 μm^2 section of a CHF cell showing the leading lamella. The image in *A* was taken with the focal plane coincident with the base of the CHF cell. For each of the following images (*B–H*), the focal plane was moved up (dorsally) 1 μm. Images were taken at 1.0 s intervals. The arrow in *D* shows a region in which the ruffle extended parallel to the direction of optical shear, and hence where little image contrast is seen. In *H* are plotted the lines that define the cross-sectional planes that were used in defining the shapes of the ruffles in cross section (Fig. 5). The dark line that follows the center of the ruffling ridge in *H* represents the ridge edge contour used for three-dimensional reconstruction. A perspective drawing of outlined ridges defined for these optical sections is presented, after turning counterclockwise by 90° in *I*. The bar in *H* represents 10 μm.

and steadily, as suggested previously by time lapse films. The extension data in Fig. 2 *B* were fitted by least squares to straight lines that have been included in the figure. For all of these fits, the correlation coefficients were > 0.97. When these data were fitted to a second order polynomial the reduced chi squared values for 15 of the 22 curves were not significantly decreased. For the seven curves that were improved, there was no preference for the second derivative of the fitted polynomial to be either positive or negative. Hence, to the resolution of the technique, which we estimate to be 0.2 μm, lamellipodia extend smoothly and monotonically with constant velocity, beginning and ending with rapid acceleration and deceleration.

Optical Sectioning Data

The raw optical sectioning image data for one time frame for one cell are presented in Fig. 3. Pictured here are 30 × 30-μm sections of the cell that include the leading lamella. In Fig. 3 *A*, the focal plane is set to view the base of the cell. Succeeding images were recorded at 1.0-s intervals with the focus plane elevated 1 μm for each interval. The long, U-shaped ruffling ridge for this cell is clearly visible. Note that there

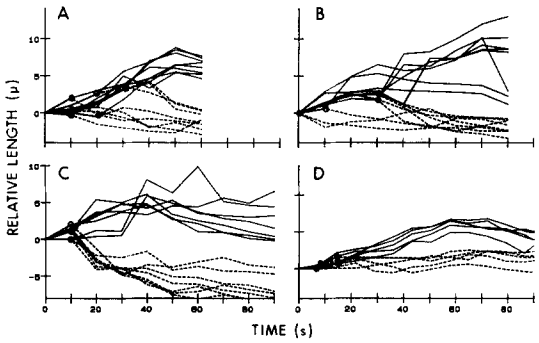

Figure 4. Lengths of ruffles. The lengths of ruffles along the planes of cross section for three different ruffles are plotted as a function of time. Solid lines represent this length. Dotted lines represent the length of the cell extension that remained in the lowest focal plane; that is, within ~0.3 μm of the base of the cell. Circles indicate the points at which the ruffles first noticeably lifted off the substratum. *A* plots the lengths of the cross-sectional shapes for the U-shaped ruffle shown in Fig. 3, and plotted in cross section in Fig. 5 *A*. *B* and *C* plot the lengths for the ruffles whose cross-sectional shapes are plotted in Fig. 5 *B* and *C*, respectively. *D* plots the lengths of one ruffle observed at 25°C, the cross-sectional shapes of which are plotted in Fig. 5 *D*.

is little crossover from section to section. Each image displays a separate view of the ruffle with little interference from parts of the cell that are out of focus. This is due to the high numerical apperture of the objective and condenser (yielding a depth of field of 0.2 μm), and to the nature of Nomarski DIC optics (Allen et al., 1969), which greatly reduces the contribution of objects outside the focal plane region to picture contrast (cf Agard, 1984). After identification of the cell edge in semiautomatic fashion, cell outlines could be put together in perspective to reconstruct the shapes of the ruffles. This kind of reconstruction is shown in Fig. 3 *I*, for the set of optical sections of Fig. 3 (turned 90°).

Lengths of the Ruffles in Cross Section

The cross-sectional lengths of the ruffles at 37°C were analyzed as a function of time (Fig. 4, *solid lines*) for three cells observed at 37°C (4, A–C) and for one cell observed at 25°C (Fig. 4 *D*). These were calculated from the raw cross-sectional data. The length of the extension of the cell in the lowest, most ventral section (within ~0.3 μm of the substrate) are plotted in this figure as the dotted lines. The average rates of extension after the ruffles were first seen to lift from the substrate are presented in Table I. After the extending lamellipodia lifted upward to form ruffles, the outer extensions of the cells near the substrate plane (within the lowest optical section) moved toward the cell centers (Fig. 4, *dotted lines*). The average rates of these retractions of the bases of the cells after ruffle lifting are also presented in Table I. (See Materials and Methods for a description of these calculations.) Although the uncertainty in the assessment of the lengths of the ruffles was high, the dispersion of measured rates of extension was not higher than that of the measured rates of base retraction. Further, the amount of increase in length of the ruffles after lifting was 4–5 μm, much higher than the 0.7–1.5 μm estimated uncertainty of individual measurements. We conclude that after a lamellipodium has bent and lifted up away from the substrate, its length increases at an average rate that is nearly the same as its rate of extension when it was parallel to the substratum (Fig. 2 *C*). Further, we conclude that the leading portion of the cell, which remains near the substrate after the ruffle has lifted, is retracted toward the cell center at a slower rate.

Cross-sectional Shapes

Fig. 5 presents vertical cross sections of ruffles at different points along their breadths. The shapes of the ruffles for the different time frames are overlaid, and the time sequence is noted in the figure. These shapes have been corrected for time slurring resulting from the 1-s time lag between the recording of successive images that make a single time frame (see Materials and Methods).

These drawings show that the lifted ruffles are not uniformly curved but remain very nearly straight over most of their length and bend sharply about hinge points near their attachment to the substratum. At times long after the ruffle was raised, however, the shape was sometimes crinkled (see Fig. 5, *B* and *C*). The speed of the tip of the ruffle often reached 0.2–0.4 μm/s.

In hopes of better observing the ruffling motion by slowing it down, three ruffles were analyzed at 25°C. The cross-sectional lengths for one of these ruffles is presented in Fig. 4 *D*, and the time-corrected cross-sectional shapes for this ruffle are presented in Fig. 5 *D*. The average rates of extension of the length of the ruffle and of retraction of the base of the ruffle after lifting are summarized in the last line of Table I. These ruffles were somewhat smaller than those observed at 37°C and did not lift or swing as quickly. The reduction in the speed of lamellar elevation permitted improved analysis of the shape changes of the ruffle because of effectively improved time resolution. The data support the conclusions reached from the 37°C data. Clearly, the extending lamellipodia continued to lengthen as they bent upward. The base of the one cell examined quantitatively (Fig. 4 *D*) did not move detectably toward the cell center, however. Again, similar to the 37°C data, lifted ruffles were straight in cross section.

Table I. Rates of Lamellar Motions

Before lifting	Lamellar extension	
	5.3 ± 1.0 (21)‡	
After lifting	Rate of extension	Rate of base retraction
Cell A	6.8 ± 2.6	3.7 ± 2.1
Cell B	6.5 ± 3.7	2.1 ± 3.2
Cell C	7.6 ± 5.3	4.9 ± 2.6
Cell D (25°C)	7.6 ± 2.7	0.3 ± 2.0
Average for cells A–C	7.0 ± 3.9 (18)§	3.6 ± 2.8 (18)§

* Rates of lamellar extension before lifting (data of Fig. 2 *B*) and ruffle extension and base retraction after lifting (data of Fig. 4). All in μm/min.
‡ Standard deviation, with the number of measurements, each on a different ruffle, shown in parentheses.
§ Standard deviation, with total number of measurements (six from each of the cells *A–C*).

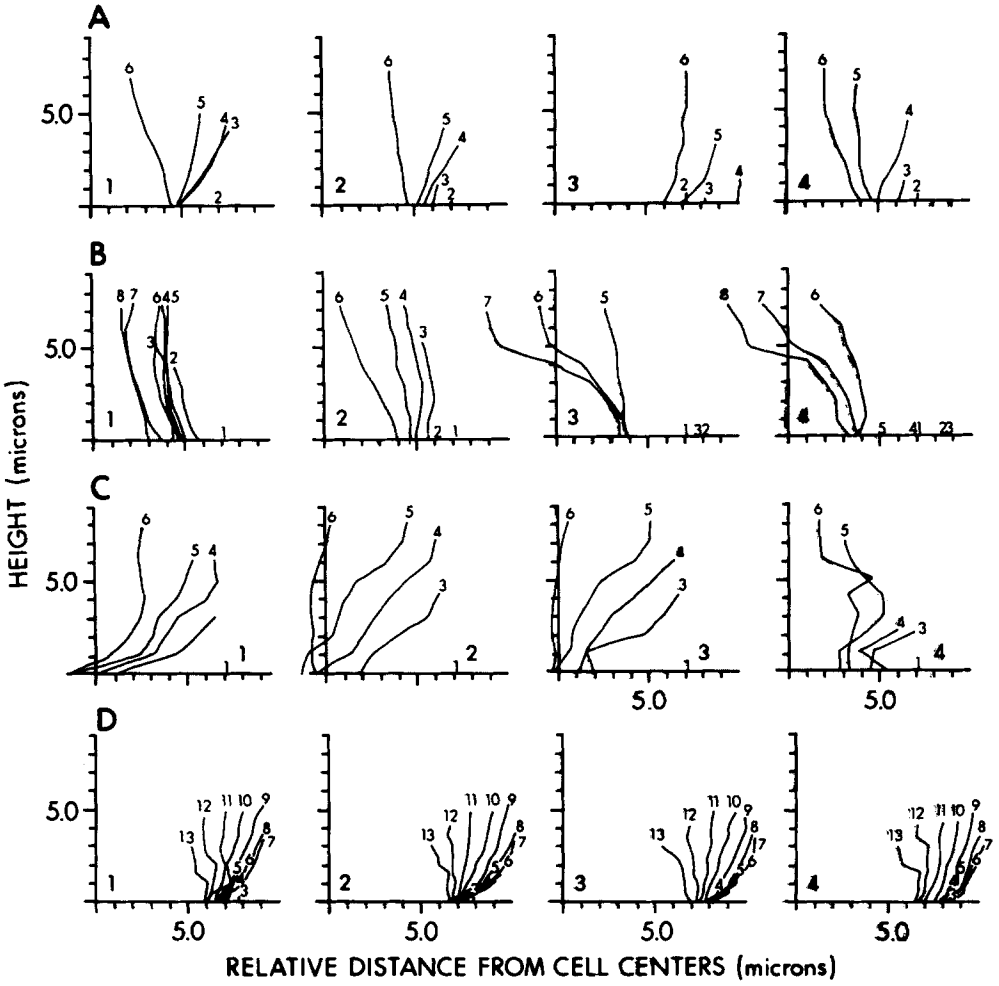

Figure 5. Ruffle cross sections. The cross-sectional shapes of three different ruffles observed at 37°C (*A*, *B*, and *C*) and for one ruffle observed at 25°C (*D*) corrected for the time lag between acquisition of image sections are plotted, with time frames overlaid and numbered in sequence. *A* presents the cross-sectional shapes for four planes of cross section spaced out along the curved edge of the leading lamella pictured in Fig. 3. *B–D* present cross sections spaced out along three different ruffles. Successive time frames for *A–C* were separated by 10 s. Time frames for *D* were separated by 7.2 s (and optical sections for this cell were taken 0.6 s apart).

Deformation of Ruffles and Their Recovery

The fact that ruffles remain largely straight in cross section after lifting suggests they are stiff structures. We, then, used quartz fishpole probes to exert force on ruffles and to measure the force with which they resisted deformation. The resisting force exerted by the ruffle was determined by measuring the bending of the probe. Only the deformability of large ruffles, which formed smooth, long (up to 10 μm) ridges parallel to the edges of the cells, were tested. These were contacted as near the tips of the ruffles as possible, and were pushed perpendicular to their long axis either away from or toward the cell center. Since these ruffling ridges generally spontaneously fold back toward the center of the cell (Abercrombie et al., 1970*b*), the push out was against and the push in was with the normal direction of motion for these structures.

Fig. 6 presents an example of a ruffle first pushed inward and then outward. Notice that the shape of the ruffle did not change very much; the ruffle bent as a unit. This was found to be true for all deformations made. The ruffling ridge generally bent about an axis located approximately at the base of the ruffle and parallel to the substratum and the edge of the cell.

In most experiments, the deformed ruffles recovered their shape very rapidly after removal of the fishpole probe. As the probe slipped off the ruffles at the end of a sweep, the ruffles sprang back most of the way to their prestressed positions in about one-fourth of a second, as determined from the time lapse video recordings. This is displayed in video frames 18 and 25 of Fig. 6. This rapid recovery was observed for both inward and outward deformations. The dotted lines drawn in these frames represent the shape of the ruffle in the previous frames, 17 and 24, respectively. Since deformations ranged up to 5 μm, this recovery involved a very fast motion. The speed and extent of shape recovery suggest that it was dominated by elastic rather than viscous forces. In a few instances, ruffles did not recover from very large deformations. For all structures, however, ruffle retraction, as observed by time lapse recording (data not shown), continued even after several deformations. This was true even for two ruffles that were pushed away from the cell center and flattened onto the substrate. These did not recover their shape rapidly but, after slight delays, bent upwards again and resumed the ruffling activity.

Linearity of Force Versus Displacement for Ruffle Deformations

To compare different measurements, we must know the de-

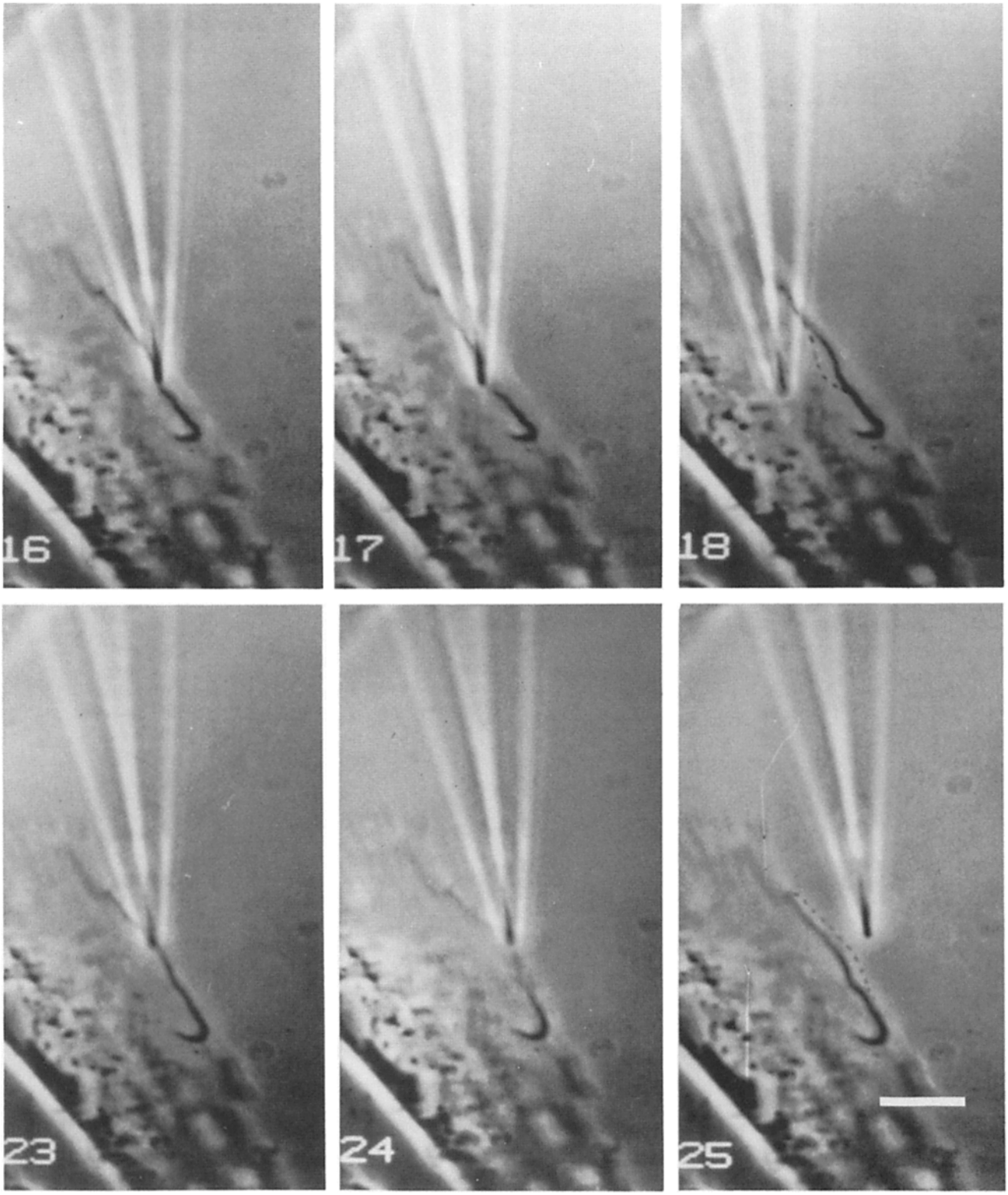

Figure 6. A ruffle pushed in and then out. One ruffle on a BC3H1 cell was pushed in toward the center of the cell in video frames 16 and 17, and then released before frame 18 to spring back outward. 5 s later the same ruffle was pushed outward away from the center of the cell in video frames 23 and 24, and was released before frame 25. The dotted lines in frames 18 and 25 represent the shapes of the ruffle in the previous frames under stress, frames 17 and 24, respectively. Frames were recorded at 1 s intervals. Bar, 5 μm.

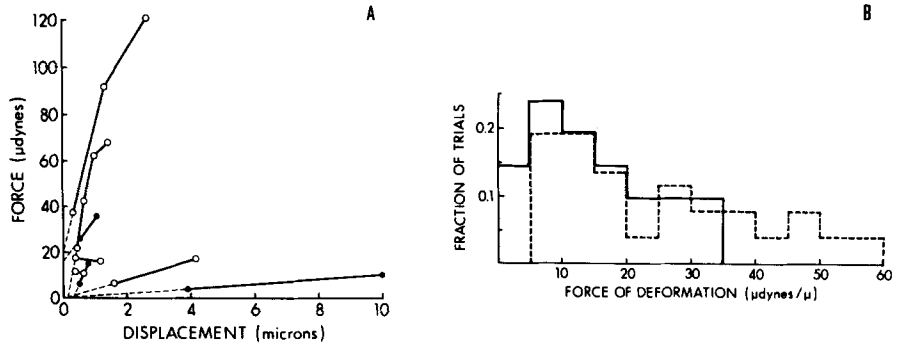

Figure 7. Force versus deformation. Plotted in Fig. 7 *A* are all trials performed on the CHF cells in which successive video frames showed a sequence of measurements of force as a function of the amount of deformation. Data from successive frames showing measurements on the same ruffle with progressive amounts of deformation are connected by straight, solid lines. Dashed lines show how these lines would extrapolate back toward zero force and zero deformation. Open circles represent ruffles that were pushed out, and closed circles represent ruffles pushed in. Similar data were obtained for the BC3H1 cells (not shown). Generally force scaled linearly with deformation, except for smaller deformations where signal to noise was low. In Fig. 7 *B*, the distribution of measured forces of resistance to deformation for both CHF and BC3H1 cells are plotted. The fraction of total trials measured within each range of force per unit of deformation is plotted as a function of the force per unit of deformation. Dotted lines represent the distribution for ruffles pushed outward (n = 26), and solid lines represent that for ruffles pushed inward (n = 21).

pendence of the force on the amount of deformation. The data for all ruffles tested on CHF cells for which successive force/displacement measurements (in successive frames) were recorded are plotted in Fig. 7. Measurements for individual are ruffles are connected by lines. To good approximation, the resisting force was a linear function of the size of the deformation and extrapolated back to near zero force at zero displacement. This relation, however, did not always hold (see examples in Fig. 7) as a result, most likely, of the low signal to noise ratio. This held equally well for ruffles pushed out (away from the center of the cell) and for ruffles pushed in. Hence measurements can be characterized and compared in terms of the average force per unit of deformation measured.

Forces of Deformation for Ruffles

The values obtained for the forces of deformation of ruffles in both BC3H1 and CHF cells are presented in Table II. The large number of measurements, ranging from 10 to 14 for each cell and direction, were taken because of the wide spread in the data. Listed measurements are the average force per unit of deformation measured for each ruffle. Most ruffles were measured two or three times, either in successive frames as presented in Fig. 7 or with multiple sweeps, for which the resting shape was different.

The ruffles for both cell types resisted deformations with a force of 15 to 30 μdyn/μm of deformation. It appeared that the ruffles resisted deformation with greater force when pushed out (against their normal direction of motion) than when pushed in. For BC3H1 cells, the measured average force resistant to an outward deformation was twofold greater than that for an inward deformation. For CHF cells, this ratio was ~1.3. A histogram of the force measurements in Fig. 8 characterizes the difference between outward and inward resistance. To facilitate comparison, data from the two cell types have been pooled. There is a non-Gaussian, skew distribution for these measurements, and hence a simple t test cannot be used to decide whether the difference is significant. Some of the difference in deformability for outward and inward pushes may have been due to the natural centripetal movement of the ruffles, which could range up to 0.2–0.4 μm during a measurement. This motion would cause us to overestimate the amount of deformation of the ruffle caused by the probe itself when pushed in, and underestimate it when pushed out. Since deformations made were usually between 1 and 2 μm (see Fig. 7), the forces of deformation could have been inaccurate by 10–30% in the two different directions.

Strictly speaking, since ruffles deformed largely at their bases, the measurements of deformability would better have been made as torques and angular displacements. In fact, pushing on ruffles at different distances from their bases may have contributed to the relatively large dispersion in the measurements. Unfortunately, our experimental procedure did not provide for a direct measure of the distance between the point of application of force and the hinge about which the ruffle bent. We estimate that the force was applied to a ruffle 7–10 μm from its base and that the direction of force was mainly perpendicular to the plane of the lamella. The average value of 20 μdyn/μm of displacement converts to an estimated average angular deformability (torque per unit of angular deformation) of 1.4 μm-mdyn/radian.

Table II. Forces of Deformation

Cell type	Pushed out*	Pushed in*
BC3H1	28 ± 14‡ (14)§	14 ± 7 (13)
CHF	20 ± 16 (14)	15 ± 12 (10)
Total	24 ± 15 (SE = 2.9)‖	15 ± 10 (SE = 2.0)

* All units, in μdyn/μm.
‡ Standard deviation of the distribution.
§ Number of separate structures tested.
‖ SEM.

Traction on the Leading Lamella

The measurement of ruffle deformability provides information about the structural strength of the ruffle, but not about the force that can be generated by the ruffle or by the leading lamellas of these cells. On an active cell particles picked up at the leading edge (where the ruffle occurs) are transported back along its dorsal and ventral surfaces across the broad, thin leading lamella to a region anterior to the nucleus (Abercrombie et al., 1970*c*; Dembo and Harris, 1981; Sheetz et al., 1989), suggesting that centripetal forces are being generated. We observed centripetal movement of our quartz fish-

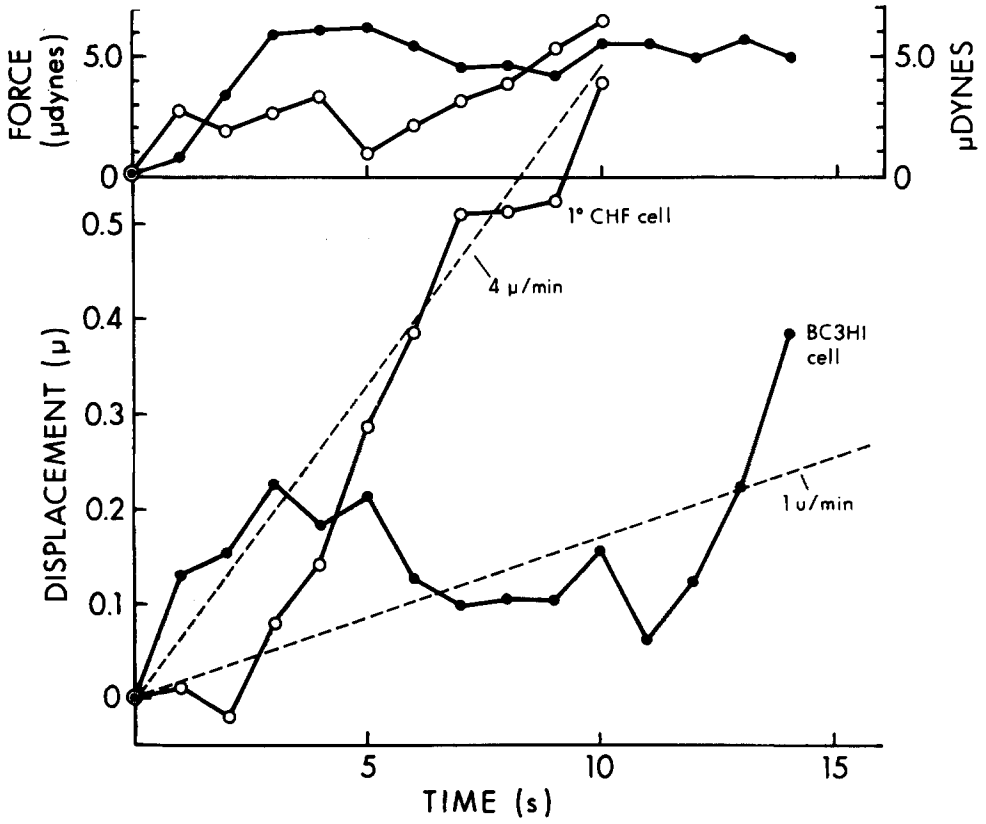

Figure 8. Lamellipod pulling. The ability of a BC3H1 cell and a CHF cell to pull the fishpole probe toward the cell center is plotted. The probe tip contacted the cells on the leading lamella behind the ruffling edge. Filled and open circles designate the forces exerted on BC3H1 and CHF cells, respectively. (*Lower panel*) The displacement of the tip of the fishpole probe (in micrometers) in a direction toward the centers of the cells is plotted as a function of time. The dashed lines plot an average velocity of 1 and 4 μm/min for reference. (Upper panel) The force resisting that displacement exerted by the fishpole probe (μdyn) is plotted as a function of time.

pole probes resting on the leading lamellas, and have attempted to measure the centripetal force that drives this motion. The tip of the fishpole probe was brought down to touch the cell surface, and the pipette holding the moored end of the fiber was lowered another 5–10 μm with no noticeable change in the position of the tip. This translates to the probe pushing down on the cell with a force of roughly 15 μdyn. Since spread cells resist indentation with a force in the range of 1 mdyn/μm for a probe of roughly the same dimensions (Petersen et al., 1982), this downward force would be expected to produce a deformation on the order of 0.01 μm into the surface of the cells. The fishpole probe was moved perpendicular to its long axis away from the cell center during the measurements in an attempt to counterbalance the force inward exerted on the probe by the cell and thereby obtain approximately a static force measurement.

The force exerted outward by the probe and the movement inward of the probe tip are plotted in Fig. 9. For the measurement of the BC3H1 cells, the outward force of the probe was maintained at 5 ± 1 μdyn for most of the 14 s of the experiment. The cell overcame this nearly steady outward force and pulled the probe tip toward its center with an average velocity of 1.5 μm/min. If the tip were sliding to some extent along the surface of the cell during the experiment, this would be an underestimate of the rate of motion of the cell surface. For the CHF cell, the force exerted against the inward movement by the fishpole probe was gradually increased over the 10 s of the experiment, and reached a similar value of 5 μdyn. The probe tip was pulled in at a rate of ~4 μm/min. The probe came into contact with the base of a ruffle that was retracting inward at about the fifth second of the experiment. For both trials, the force of bending of the

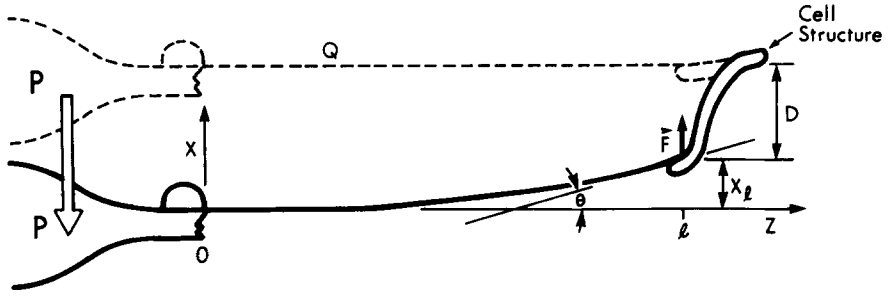

Figure 9. Geometry of force measurement. The fishpole probe consists of a quartz fiber (*f*) glued onto the broken end of a glass micropipette (*p*) with a small drop of epoxy. The probe is drawn in two positions. In the upper position the probe extends along the *Z* axis just touching an object (*o*) without exerting force on it. The origin of the *Z* axis has been placed at the fastened tip of the quartz fiber, and the fiber has a length *L*. In the lower drawing, the micropipette has been moved down a distance, -*X*, and the tip of the probe has deformed the object by an amount, *D*. The probe has been bent so that the tip of the probe forms an angle, θ, with the *Z* axis. The angle, θ, is measured, and the amount of displacement of the quartz fiber's tip, *X*-*D*, and hence the force, *F*, on the tip are calculated as described in the Appendix I.

probe was not sufficient to stop the progress of the tip completely. Hence, the leading lamella can move the probe inward with a force at least as great as that which we have measured, but this may not be the maximal force that can be generated. Attempts to resist motion with larger force, however, resulted in the probe sliding off the cells.

Discussion

We have studied the extension and retraction of the leading edge of locomoting fibroblasts by high resolution light microscopy and analysis of digitized video images. We have demonstrated that lamellar extensions begin randomly in time and occur with constant velocity of extension both before and after the lamellas bend upward to form ruffles. Further, we have shown that the ruffling lamellas are straight in cross section, quite stiff and elastic, and appear to be subject to relatively large retractive forces. Our observations allow us to draw conclusions about the mechanisms and mechanics of these processes.

Extension of the Lamellipodium

We have observed that the leading edge of a locomoting fibroblast extends as a broad, flat sheet or lamellipodium at rates of 2–7 μm/min, in agreement with previous estimates of from 2 to 8 μm/min (Abercrombie et al., 1970*a*; Chen, 1979). Most of the active lamella extends with the same velocity and to the same extent. Most informative is the observation that the velocity of extension remains constant during most of its duration within the resolution of our measurements and that the extension reaches a maximal velocity quickly; i.e., the period of acceleration to constant velocity is very brief.

Viewed a priori, the rate of lamellar extension could be determined by a balance between the forces driving the extension and those resisting it, or, if the resisting forces are negligibly small by the rate of application of the extending forces. If lamellar extension were limited by a balance between driving and resisting forces, its rate could depend on the rate of application of the former and the dependence of the latter on the size and shape of the lamellipodium. A simple linear viscoelastic model predicts an exponential time course for lamellar extension and so is contradicted by the experimental observations. This model, although rudimentary helps to clarify the various contributions to the force balance and is discussed in greater detail in Appendix II. As another example, the time course for acrosomal extension (Tilney and Inoue, 1982) has recently been explained in terms of a changing balance between viscoelastic forces which resist acrosomal extension and osmotic forces which drive it (Oster et al., 1982; Tilney and Inoue, 1985; Oster and Perelson, 1987). This model yields a dependence on $t^{-1/2}$, in agreement with their experimental observations. A similar model has been suggested to account for lamellipodial extension (Oster and Perelson, 1985). Interestingly, the time course for the extension of filopodia in nerve growth cones, although much slower, qualitatively resembles that of the Thyone acrosomal process (Argiro et al., 1985). Hence, the shape of the process may play a significant role in determining its time course of extension.

None of these simple models yield a behavior consistent with our results, that extension occurs with constant velocity. Although it is possible to develop force balance models that are consistent with these observations, this requires assumptions that cannot yet be justified experimentally, such as time or shape dependent resistance to extension. Hence, it seems simplest at present to suppose that the constant rate of lamellipodial extension results from the constant rate of application of force, presumably due to the steady operation of the motor that drives it, with little effect of viscoelastic resistance. The proposed constant rate of operation of the driving motor may be controlled by a constant rate of delivery of a limiting material, or by the speed of a rate-limiting biochemical reaction.

Force for Lamellar Extension

The origin of the force responsible for lamellar extension is unclear. One possibility is an increase of intracellular hydrostatic pressure due to an osmotically driven influx of water (Tilney and Inoue, 1985). Since the hydrostatic pressure would be increased throughout the cell, this hypothesis also requires a mechanism for confining the cellular deformation to the extending lamella (cf Oster, 1988). In our opinion it is simpler to attribute tentatively the extensional force either to the polymerization of microfilaments in the lamella or to actin–myosin interactions (cf Smith, 1988; Mitchison and Kirschner, 1988). Clearly, polymerization of proteins can produce sufficient force to deform membranes as demonstrated by the deformation of erythrocytes by sickle cell hemoglobin (Mozzarelli et al., 1987) and recent observations of the deformation of lipid vesicles by the polymerization of enclosed actin (Cortese et al., 1989). The observations that rhodamine-labeled filamentous actin does not move out into an extending process (Felder, 1984; Wang, 1985) and that freshly microinjected monomeric rhodamine-labeled actin is preferentially incorporated into the extending lobopodia of amoebae (Taylor et al., 1980) are consistent with this interpretation. The rate of polymerization might be limited by the concentration either of actin monomer or of filament ends or, in a more complex manner by specific actin binding proteins or ion fluxes. If these remained effectively constant, the polymerization rate and the consequent rate of application of extensile force would also be constant. If both viscous and elastic resistance to extension were negligible, then the rate of extension would be determined by the unloaded (maximal) rate of polymerization. The rapid diffusion of actin in cytoplasm (Kreis et al., 1982; Felder, 1984) is sufficient to provide a steady state monomer concentration and therefore constant rate of polymerization, but actin polymerization in living cells is not well enough characterized to assess this assumption. Alternatively, extension due to interaction of myosin (presumably myosin I; cf Mitchison and Kirschner, 1988), attached to the lamellar membrane, with actin filaments anchored to a fixed position relative to the substrate, could produce lamellar extension with constant velocity. Recent observations of rapid forward transport of membrane glycoproteins in the lamellas of rapidly translocating fish epidermal keratocytes are consistent with the generation of forward extensile forces (Kucik et al., 1989).

Ruffle Elevation

As it extends, the lamellipodium begins to bend upward to form a ruffle at a point 2–4 μm behind its advancing tip. The

outward extension of the elevating ruffle continues at its initial rate until it has swung past vertical, typically 40–60 s after beginning to bend upward. Hence, the initiation of bending is not correlated with cessation of extension. The bending its confined to a narrow region of high curvature, the "hinge," near the base of the ruffle, leaving most of the ruffle straight in vertical cross section (cf. Abercrombie et al., 1970*b*). When pushed with a probe, a ruffle similarly bends at its base, resisting the imposed stress with forces of up to and beyond 50 μdyn, and then springs back rapidly after the probe is removed to continue its natural movement. Hence, the ruffles seem to be quite stiff for such thin structures and largely elastic. That the ruffles remain straight while growing in length after elevating suggests that the shape of the lamellipodium is intrinsic to its structure and not merely a consequence of its development in juxtaposition to the flat surface of the substratum. The observed stiffness indicates that the material properties are determined by cytoskeletal structures rather than by the membrane. The ability of phospholipid membranes to sustain shear or bending strain is far too small to resist deformations with the forces that we have measured (Evans and Hochmuth, 1978). The stiffness and elasticity of fibroblast lamellipodia is reminiscent of the similar characteristics of neutrophil pseudopodia observed by micropipette aspiration (Schmid-Schoenbein et al., 1982).

Force for Ruffle Bending

The origin of the force that bends a lamella upward to form a ruffle is unknown. We assume that to bend the ruffles naturally, the cell must exert a torque similar in magnitude to the torque we have exerted in bending the ruffles with our quartz probe. (This may not be true, however. For example, the ruffle could be bent in only small increments requiring much less force, with rapidly coupled bending and cytoskeletal remodelling to relieve stress.) Because of the magnitude of the force required, we favor actin–myosin interactions exerted through the actin filaments within the lamella. To bend the lamella requires the exertion of a torque about the hinge axis and therefore a component of force acting on the lamella perpendicular to this axis exerted some distance from the axis and normal to the plane of the lamella. The geometry of the extended lamella is highly inefficient for this function. The lamellas are very thin and so the filaments must be largely parallel to the lamellar plane. Further, they may exert force on the whole surface of the lamella. Thus, only a small component of the force is applied perpendicular to the lamellar plane and is exerted with an effective radius substantially less than the full height of the ruffle. In our measurements, however, the probe was applied to the tip of the ruffle, and the full force was applied perpendicular to the lamellar plane. Hence, we estimate that the natural retraction force exerted on the lamellipodium is substantially greater (perhaps >10-fold) than the force with which we were able to bend ruffles.

Surface Traction Forces and Implications for Cell Locomotion

The measurements discussed above place constraints on models both of lamellar motion and of the generation of force within lamellas. Ultimately, however, we want to know how these motions and forces are related to cell locomotion. Without a more complete description of the geometry, the origin of driving forces, and the nature of forces resisting cell motions interpretations remain speculative. To provide a working hypothesis and in agreement with suggestions of others (Abercrombie et al., 1977), we suppose that the forces which create and move ruffles are the same forces that drive cell movement. In this view, the leading lamella is extended to develop more forward contacts with the cell's surroundings. As the lamella extends, fairly strong retractive forces are exerted, possibly by interaction of myosin and actin filaments. The retractive forces either pull the lamella rearward and bend it upward (for cells attached on one side to a flat surface), or, if the lamella is more firmly attached to the substrate, draw the rearward portions of the cell forward to prepare for a further cycle of lamellar extension (cf Chen, 1979, 1981). From this perspective, the ruffle deformability measurements discussed above should relate directly to the retractile forces that pull the cell forward.

Our direct measurements of surface retraction forces yield values that approximately agree with forces which resist ruffle bending. This supports the contention that the same forces are responsible both for ruffle elevation and for forward cellular retraction during locomotion. The dynamic, retractive force is ~5 μdyn/μm² of probe surface in contact with the cell surface. This is two orders of magnitude greater than the force estimated to be required to transport particles rearward along the leading lamella of CHF cells and mouse peritoneal macrophages (Dembo and Harris, 1981). This discrepancy presumably indicates that the rate of particle transport is determined by the rate of the motor that drives transport and is not influenced by the small viscous resistance to the particle motion.

The measured force of surface retraction is in the range of pressures required for elastic shear (~10^3 dyn/cm²) but is 100-fold less than that required for elastic stretching (~10^5 dyn/cm²) of erythrocyte membranes (Evans and Skalak, 1980). The retractive force is also considerably less than the forces developed in stress fibers spanning focal contacts (Izzard and Lochner, 1980). This static tensile force has been estimated to be on the order of 10 mydnes for a fibroblast with a leading edge 10 μm in length (Harris et al., 1980). In contrast, cells which crawl more rapidly like polymorphonuclear leukocytes and macrophages do not develop stress fibers or focal contacts (Oliver et al., 1978; Painter et al., 1981). For these cells, a retractive force of 5 to 50 μdyn exerted near the leading edge may be enough to pull the cells forward. The drag forces acting on these cells as well as the retractive force produced at their leading edges, however, remain to be measured.

In summary, our measurements of the rates of lamellar extension and the shapes and deformability of ruffles suggest that the forces driving motion of the leading lamella are substantially larger than the forces that resist motion. Hence, the rates of movement appear to be determined by the rates of application of force. Furthermore, the forces that we have measured that resist lamellar deformation and retract the upper cell surface appear strong enough to be directly involved in forward motion of the cells. Information on the details of filament polymerization and the operation of motor proteins

within lamellas as well as characterization of other relevant forces, the force of lamellar extension and drag forces resisting motion for rapidly moving cells, for example, will allow a more definitive description of these processes.

We are grateful to Dr. Richard Wrenn for many helpful discussions and assistance with video digitization methods and to Michael Scott for the development of programs for collection and handling of digital video data.

This work was supported by National Institutes of Health grants GM 30299, GM 27160, and GM 38838, and by a grant from the Edward Mallinckrodt, Jr. Foundation.

Received for publication 28 February 1990 and in revised form 4 September 1990.

Appendix I

Bending of the Fishpole Probe as a Measure of Applied Force

The bending moment of a beam is related to the Young's modulus for the material, E, the moment of inertia of the beam cross section, I, and the radius of curvature, R, by the equation $M = EI/R$; where R is defined as

$$1/R = (d^2x/dz^2)/[1 + (dx/dz)^2],$$

which for small curvatures (i.e., where $dx/dz << 1$) becomes $1/R = d^2x/dz^2$.

For the static case of a uniform beam held fixed and straight at one end while a force F is applied perpendicular to the long axis of the beam at the other end, the bending moment M is balanced at all points along the beam by the force component $M = F(l-z)$; where l is the length of the beam and z is the distance along the beam. This situation along with a description of the axes is pictured in Fig. 9. Substitution yields:

$$d^2x/dz^2 = F(l-z)/EI.$$

The solution to this equation for the boundary conditions already stated ($x = 0$ at $z = 0$ and $dx/dz = 0$ at $z = 0$ is):

$$x = F/(EI)\ [1/2\ lz^2 - 1/6\ z^3]. \quad (1)$$

The deflection at the tip of the beam (x_l) and the slope at the tip $(dx/dz)_l$ are

$$x_l = Fl/3EL \quad (2)$$

$$(dx/dz)_l = -Fl/2EL;$$

hence,

$$x_l = -2/3\ l\ (dx/dz);$$

or

$$x_l = -2/3\ l \sin\theta; \quad (3)$$

where the angle θ is the difference in direction of the probe tip for stressed and unstressed conditions (as in Fig. 9).

Thus, the deflection of the tip of the beam is proportional to the applied force F (Eq. 2) and can be measured by measurement of the tip angle θ (Eq. 3), and the sensitivity of the beam (that is the amount of tip displacement per unit of applied force) is proportional to l (Eq. 2).

Appendix II

Simple Mechanism for Lamellar Extension

Balance of Forces. We treat the lamella as the simplest one-dimensional linear viscoelastic solid, a Voigt solid represented by an elastic element, a spring, in parallel with a viscous element, a dashpot. As the lamella extends, the former generates a force $-kx$; the latter, a force $-\eta dx/dt$, where x is the degree of extension of the lamella from its condition of mechanical equilibrium, and k and η are elasticity and viscosity coefficients, respectively. Then the forces resisting extension are $F(t) = -kx - \eta dx/dt$. If we further suppose the sudden application of a constant extensional force, F_0, then the lamellar extension should follow the time course, $x(t) = -(F_0/\kappa)\ [1 - \exp(-t/\tau)]$ where $\tau = \eta/\kappa$. This model, and also more complicated one-dimensional linear viscoelastic solid models, thus predict an exponential time course of lamellar extension inconsistent with our results. A constant rate of extension can be recovered from this model by supposing that the lamella behaves as a viscous fluid with negligible elastic resistance; i.e., $\eta >> \kappa$. As indicated in the text, however, evidence from our measurements and those of others suggests that the lamella is more likely to behave as an elastic solid than a viscous fluid.

The forces resisting extension might depend on the degree of extension. For example, if the viscous resistance developed uniformly throughout the extending lamella, then η might be proportional to the degree of lamellar extension, $\eta = cx$, where c is a constant, as previously supposed for the thyone acrosomal process (Oster et al., 1982). For this latter situation $-t/\tau' - x(t) + x_{eq} \log[|1 - x(t)/x_{eq}|]$ where we have supposed that the lamella extends in response to a constant force, F_0, and $x_{eq} = F_0/k$ and $\tau' = c/k$. This model does not predict a constant velocity of lamellar extension. If the elastic resistance were negligible, then the model becomes similar to that developed by Oster et al. (1982) for the Thyone acrosomal reaction. In both cases, $x^2(t) \sim t$. Although this is true for the acrosomal reaction, this relationship is contradicted for lamellar extension by our experiments.

Unloaded Extension

Another possibility is that the viscous resistance to extension is very small, as was observed for ruffle bending. Then the lamella should respond instantaneously to the extensional driving force and so the rate of extension of the lamella would be governed by the rate of application of force. More generally, if $F(t) = \alpha t$, where α is the rate of application of force, then, for the Voigt model considered above, $x(t) = (\alpha/k)\ [t - \tau(1 - \exp)(-t/\tau)]$. So that for times long compared to τ, the lamella would extend at a constant rate $dx/dt = -\alpha/k$. This would be preceded by an exponential approach to the constant asymptotic extension rate. If η, and therefore τ, were small, as expected from our studies of lamellar bending, this transient exponential phase might be too brief to detect. Hence our experimental results are consistent with a simple linear model in which the force is applied at constant rate.

References

Abercrombie, M., J. E. M. Heaysman, and S. M. Pegrum. 1972. Locomotion

of fibroblasts in culture IV. Electron microscopy of the leading lamella. *Exp. Cell Res.* 67:359–367.

Abercrombie, M., G. A. Dunn, and J. P. Heath. 1977. The shape and movement of fibroblasts in culture. *In* Cell Tissue Interactions. J. W. Lash and M. M. Burger, editors. Raven Press, New York. 57–70.

Abercrombie, M., J. E. M. Heaysman, and S. M. Pegrum. 1970*a*. The locomotion of fibroblasts in culture I. Movements of the leading edge. *Exp. Cell Res.* 59:393–398.

Abercrombie, M., J. E. M. Heaysman, and S. M. Pegrum. 1970*b*. The locomotion of fibroblasts in culture II. Ruffling. *Exp. Cell Res.* 60:437–444.

Abercrombie, M., J. E. M. Heaysman, and S. M. Pegrum. 1970*c*. The locomotion of fibroblasts in culture III. Movements of particles on the dorsal surface of the leading lamella. *Exp. Cell Res.* 62:389–398.

Agard, D. A. 1984. Optical sectioning microscopy: cellular architecture in three dimensions. *Annu. Rev. Biophys. Bioeng.* 13:191–219.

Allen, R. D., G. B. David, and G. Nomarski. 1969. The Zeiss-Nomarski differential interference equipment for transmitted-light microscopy. *Z. Wiss. Mikrosk. Mikrosk. Tech.* 69:193–221.

Argiro, V., M. B. Bunge, and M. I. Johnson. 1985. A quantitative study of growth cone filopodial extension. *J. Neurosci. Res.* 13:149–162.

Bray, D., and J. G. White. 1988. Cortical flow in animal cells. *Science (Wash. DC).* 239:883–888.

Bretscher, M. S. 1984. Endocytosis: relation to capping and cell locomotion. *Science (Wash. DC).* 224:681–686.

Chen, W. -T. 1979. Retraction-induced spreading during fibroblast movement. *J. Cell Biol.* 81:684–691.

Chen, W. -T. 1981. Mechanism of retraction of the trailing edge during fibroblast movement. *J. Cell Biol.* 90:187–200.

Cole, K. S. 1932. Surface Forces of the Arbacia Egg. *J. Cell Comp. Physiol.* 1:1–9.

Cortese, J. D., B. Schwab, III, C. Frieden, and E. L. Elson. 1989. Actin polymerization induces a shape change in actin-containing vesicles. *Proc. Natl. Acad. Sci. USA.* 86:5773–5777.

Dembo, M., and A. K. Harris. 1981. The motion of particles adhering to the leading lamella of crawling cells. *J. Cell Biol.* 91:528–536.

Dembo, M., F. H. Harlow, and W. Alt. 1984. The biophysics of cell motility. *In* Cell Surface Dynamics: Concepts and Models. A. S. Perelson, C. DeLisi, and F. W. Wiegel, editors. Marcel Dekker, Inc., New York. 495–541.

Dipasquale, A. 1975. Locomotory activity of epithelial cells in culture. 1975. *Exp. Cell Res.* 94:191–215.

Evans, E. A., and R. M. Hochmuth. 1978. Mechanochemical properties of membranes. *Curr. Top. Membr. Transp.* 10:1–64.

Evans, E. A., and R. Skalak. 1980. Mechanics and Thermodynamics of Biomembranes. CRC Press, Inc., Boca Raton, FL. 254 pp.

Evans, E. A., R. Kwok, and T. McCown. 1980. Calibration of beam deflection produced by cellular forces in the 10^{-9}–10^{-6} gram range. *Cell Biophys.* 2:99–112.

Felder, S. 1984. Mechanics and Molecular Dynamics of Fibroblast Locomotion. Ph.D. thesis. Washington University, St. Louis, MO.

Harris, A. K., P. Wild, and D. Stopak. 1980. Silicone rubber substrata: a new wrinkle in the study of cell locomotion. *Science (Wash. DC).* 208:177–179.

Howard, J., and A. J. Hudspeth. 1987. Mechanical relaxation of the hair bundle mediates adaptation in mechanoelectrical transduction by the bullfrog's saccular hair cell. *Proc. Natl. Acad. Sci.* 94:3064–3068.

Hunter, E. 1979. Biological techniques for avian sarcoma viruses. *Methods Enzymol. Cell Culture.* 58:379–393.

Ingram, V. M. 1969. A side view of moving fibroblasts. *Nature (Lond.).* 243: 641–644.

Izzard, C. S., and L. R. Lochner. 1976. Cell-to-substrate contacts in living fibroblasts: an interference-reflexion study with an evaluation of the technique. *J. Cell Sci.* 21:129–159.

Izzard, C. S., and L. R. Lochner. 1980. Formation of cell-to-substrate contacts during fibroblast motility: an interference-reflexion study. *J. Cell Sci.* 42:81–116.

Kishino, A., and T. Yanagida. 1988. Force measurements by micromanipulation of a single actin filament by glass needles. *Nature (Lond.).* 334:74–76.

Kreis, T. E., B. Geiger, and J. Schlessinger. 1982. Mobility of microinjected rhodamine actin within living chicken gizzard cells determined by fluorescence photobleaching recovery. *Cell.* 29:835–845.

Kucik, D. F., E. L. Elson, and M. P. Sheetz. 1989. Forward transport of glycoproteins on leading lamellipodia in locomoting cells. *Nature (Lond.).* 340:315–317.

Kupfer, A., and S. J. Singer. 1988. Molecular dynamics in the membranes of helper T cells. *Proc. Natl. Acad. Sci. USA.* 85:8216–8220.

Lowry, O. H., and J. V. Passonneau. 1972. A Flexible System of Enzymatic Analysis. Academic Press, New York, NY. 236–249.

Mitchison, T., and M. Kirschner. 1988. Cytoskeletal dynamics and nerve growth. *Neuron.* 1:761–772.

Mozzarelli, A., J. Hofrichter, and W. A. Eaton. 1987. Delay time of hemoglobin S polymerization prevents most cells from sickling in vivo. *Science (Wash. DC).* 237:500–506.

Oliver, J. M., J. A. Krawiec, and E. L. Becker. 1978. The distribution of actin during chemotaxis in rabbit neutrophils. *J. Reticuloendothel. Soc.* 24:697–704.

Oster, G. 1988. Biophysics of the leading lamella. *Cell Motil. Cytoskeleton.* 10:164–171.

Oster, G. F., and A. S. Perelson. 1985. Cell spreading and motility: a model lamellipod. *J. Math. Biol.* 21:383–388.

Oster, G. F., and A. S. Perelson. 1987. The physics of cell motility. *J. Cell Sci. Suppl.* 8:35–54.

Oster, G. F., A. S. Perelson, and L. G. Tilney. 1982. A mechanical model for elongation of the acrosomal process in thyone sperm. *J. Math. Biol.* 15:259–265.

Painter, R. G., J. Whisenand, and A. T. McIntosh. 1981. Effects of cytochalasin B on actin and myosin association with particle binding sites in mouse macrophages: implications with regard to the mechanism of action of the cytochalasins. *J. Cell. Biol.* 91:373–384.

Petersen, N. O., W. B. McConnaughey, and E. L. Elson. 1982. Dependence of locally measured cellular deformability on position in the cell temperature and cytochalasin B. *Proc. Natl. Acad. Sci. USA.* 79:5327–5331.

Rinnerthaler, G., B. Geiger, and J. V. Small. 1988. Contact formation during fibroblast locomotion: involvement of membrane ruffles and microtubules. *J. Cell Biol.* 106:747–760.

Schmid-Schonbein, G. W., R. Skalak, K. L. P. Sung, and S. Chien. 1982. Human leukocytes in the active state. *In* White Blood Cells, Morphology and Rheology as Related to Function. U. Bagge, G. V. R. Born, and P. Gaehtgens, editors. Martinus Nihjoff, The Hague. 21–31.

Schubert, D., J. Harris, C. E. Devine, and S. Heinemann. 1974. Characterization of a unique muscle cell line. *J. Cell Biol.* 61:398–413.

Sheetz, M. P., S. Turney, H. Qian, and E. L. Elson. 1989. Nanometre-level analysis demonstrates that lipid flow does not drive membrane glycoprotein movements. *Nature (Lond.).* 340:284–288.

Small, J. V. 1982. Organisations of actin and fibroblast locomotion. *In* Embryonic Development. Part B, Cellular Aspects. M. M. Burger and R. Wever, editors. Alan R. Liss, New York. 341–358.

Smith, S. J. 1988. Neuronal cytomechanics: the actin-based motility of growth cones. *Science (Wash. DC).* 242:708–715.

Taylor, D. L., Y. -L. Wang, and J. M. Heiple. 1980. Contractile basis of ameboid movement VII. The distribution of fluorescently labeled actin in living amebas. *J. Cell Biol.* 86:590–598.

Tilney, L. G., and S. Inoue. 1982. Acrosomal reaction of Thyone sperm. II. The kinetics and possible mechanism of acrosomal process elongation. *J. Cell Biol.* 93:820–827.

Tilney, L. G., and S. Inoue. 1985. Acrosomal reaction of the Thyone sperm. III. The relationship between actin assembly and water influx during the extension of the acrosomal process. *J. Cell Biol.* 100:1273–1283.

Trinkaus, J. P. 1984. Cells into Organs. The Forces That Shape the Embryo. Prentice Hall, Englewood Cliffs, NJ. 543 pp.

Wang, Y. -L. 1985. Exchange of actin subunits at the leading edge of living fibroblasts: possible role of treadmilling. *J. Cell Biol.* 101:597–602.